A fluorescent nanoprobe based on AIEgen: Visualization of silver ions and sensing applications in cancer cells and *S. aureus*

Na Hee Kim[a], Rae Hyung Kang[a],[b], Peter Verwilst*[c], and Dokyoung Kim*[a],[b],[d],[e],[f]

[a] Department of Biomedical Science, Graduate School, Kyung Hee University, Seoul 02447, Republic of Korea

[b] Medical Research Center for Bioreaction to Reactive Oxygen Species and Biomedical Science Institute, Kyung Hee University, Seoul 02447, Republic of Korea

[c] KU Leuven, Rega Institute for Medical Research, Medicinal Chemistry, 3000 Leuven, Belgium

[d] Department of Anatomy and Neurobiology, College of Medicine, Kyung Hee University, Seoul 02447, Republic of Korea

[e] Center for Converging Humanities, Kyung Hee University, Seoul 02447, Republic of Korea

[f] KHU-KIST Department of Converging Science and Technology, Kyung Hee University, Seoul 02447, Republic of Korea

Author information:

*Corresponding author. D. Kim (Department of Biomedical Science, Graduate School, Kyung Hee University, Seoul 02447, Republic of Korea), P. Verwilst (KU Leuven, Rega Institute for Medical Research, Medicinal Chemistry, 3000 Leuven, Belgium)

E-mail address: dkim@khu.ac.kr (D. Kim), peter.verwilst@kuleuven.be (P. Verwilst)

Abstract:

We have developed a fluorescent nanoprobe (**AgP-1**) that can detect silver ions (Ag^+) in biological media. For the first time, a hybridized structure based on AIEgen (tetraphenylethylene; TPE) and 2-(methylthio)aniline (MTA) moiety has been designed, and its unique sensing properties toward silver ions were systematically analyzed. The nanoprobe **AgP-1** has an aggregated form with weak fluorescence and showed significant fluorescence enhancement (3.7-fold) upon forming complex with silver ions. **AgP-1** has high selectivity, high

sensitivity (detection limit 6.6 ppb), a fast response time (fluorescence enhancement within 10 s), and superior biocompatibility. Visualization of silver ions in cancer cells (U87 glioblastoma) and bacteria (*S. aureus*) was also successfully demonstrated. We believe **AgP-1** holds a great potential to serve as a practical sensor for silver ions detection in biomedical applications.

Keywords:

Fluorescent probe; silver ion; aggregation-induced emission; 2-(methylthio)aniline moiety; fluorescent imaging

1. Introduction

Humans have extensively used silver (Ag) and its chemical complexes for thousands of years. They, as high-value materials, have been used in various fields such as the chemical industry, pharmaceuticals, jewelry, and electronics [1-4]. In particular, silver ions and their complexes have received significant attention from the pharmaceutical industry for their unique biological properties being antibacterial, antiviral, and antifungal [5, 6]. However, silver not removed after the manufacturing process could be absorbed into the body and induce harmful side-effects such as like liver/kidney damage and neurodegenerative disorders [7, 8]. In this sense, the importance of developing a system to selectively detect silver ions has been developed.

Several methods based on spectroscopy, electrochemistry, potentiometric titration, and plasma-mass spectrometry has been devised to detect silver ions [9-11]. However, despite advantages for silver ion detection, such methods have limitations of being highly complex, expensive, and time-consuming for sample pretreatment [12-15]. To overcome such drawbacks, fluorescence-based tools have been recently highlighted. Fluorescence-based molecular sensing probes showed many advantages; high sensitivity and selectivity, user-friendly instrumentation, low cost, and simple sample preparation steps [16-18]. Many fluorescence-based molecular probes were reported to detect silver ions. However, some limitations still remained such as [19-24], low selectivity [19, 20], low sensitivity [20, 24], no various application [9, 22, 24] (Table S1) and it is significant challenging to design a turn-on type fluorescent probe due to the fluorescence quenching property of silver ions toward fluorophore from the charge transfer process; thus, most reported probes used a turn-off response instead.

In this present work, we disclosed a turn-on type fluorescent nanoprobe called **AgP-1** that can selectively detect silver ions in biological media. For the first time, a hybridized structure of **AgP-1** was designed, which is based on TPE (tetraphenylethylene) AIEgen (aggregation-induced emission luminogens) and 2-(methylthio)aniline (MTA) moiety. The MTA moiety could be conjugated to fluorophores via imine bond formation (Type 1) or secondary amine bond (Type 2), and it could sense a specific metal ion such as copper (II) ions (Cu^{2+}), zinc (II) ions (Zn^{2+}), mercury (II) ions (Hg^{2+}), and aluminum (III) ions (Al^{3+}) by forming a coordinate covalent bond with metal ions between nitrogen and sulfur atoms within its structure (Fig. 1a) [19-24]. The metal ion sensing mechanism of MTA moiety depends on whether it forms an imine bond or secondary amine bond combined with a fluorophore. For example, a fluorescent probe (named **PTE-1**) was reported to detect mercury ions (Hg^{2+}) in 2012, which is based on the pyrene fluorophore-conjugated with MTA by imine bond, and our research team also reported a fluorescent probe for the detection of iron(III) ions (Fe^{3+}) that is based on the naphthalene fluorophore and MTA (Type 1, Fig. 1b) [24]. As follow-up research, we focused on the development of a new fluorescent probe for selective metal ion sensing and found a unique sensing property of the hybrid structure of TPE and MTA toward silver ions, which is conjugated based on the secondary amine formation (Type 2 method) (Fig. 1c). The probe (**AgP-1**) forms aggregates in aqueous solution (pH 7.4) as a fluorescence off-state due to the free rotation of MTA moiety and non-efficient stacking of TPE moiety, but its fluorescence could be significantly enhanced when **AgP-1** chelates by forming a coordinate bond between silver ions and MTA moiety (secondary amine and ortho-thiomethyl) [25]. **AgP-1** shows superior sensing properties such as (i) high selectivity towards silver ion, (ii) high sensitivity (limit of detection: 6.6 ppb), (iii) fast responsive time (turn-on response within 10 s), (iv) high biocompatibility (negligible cellular toxicity), and (v) high applicability in bio-imaging (reliable fluorescent images within cell and bacteria). We expect that **AgP-1** could be widely applied to silver-related chemical researches and biological studies.

2. Experimental Section

2.1. Synthesis of **AgP-1**

Synthesis of **AgP-1** (2-(methylthio)-*N*-(4-(1,2,2-triphenylvinyl)benzyl)aniline). 1-(bromomethyl)-4-(1,2,2-triphenylethenyl)benzene (30 mg, 0.0705 mmol) and potassium carbonate (19.486 mg, 0.141 mmol) were dissolved in dimethylformamide (DMF, 1 mL), and 2-(methlythio) aniline

(9.814 mg, 0.0705 mmol) was then added. The mixture was stirred for 12 hours at 80 °C. After being cooled to room temperature (25 °C), the mixture was quenched by adding deionized water (DI H_2O, 3 mL). The aqueous layer was extracted with ethyl acetate (EtOAc), and the organic extract was washed with brine and dried over anhydrous sodium sulfate (Na_2SO_4). After removing the solvent under vacuum, the resulting compound was purified by silica chromatography (n-hexane/EtOAc =9:1, *v/v*) to obtain **AgP-1** (yield = 43%, white solid). The melting point of **AgP-1** was measured using a thermal analysis system (TAS, melting point: 197 °C). The **AgP-1** displayed bands at 3000–2840 and 1800–1600 cm^{-1} associated with ν(C–H) of TPE backbone, ν(C–Br) stretching of the alkyl bromide at 600–700 cm^{-1}, and the stretching vibration of the secondary amine of conjugated MTA at 3350–3310 cm^{-1}, which suggested successful synthesis of **AgP-1** (Fig. S1). ^{1}H NMR (500 MHz, $CDCl_3$): δ 7.41 (dd, J = 7.4, 1.7 Hz, 1H), 7.16-7.09 (m, 12H), 7.06-7.00 (m, 8H), 6.68-6.65 (m, 1H), 6.55 (dd, J = 8.0, 1.1 Hz, 1H), 5.29 (s, 1H), 4.31 (s, 2H), 2.32 (s, 3H). ^{13}C NMR (500 MHz, $CDCl_3$): δ 207.2, 171.3, 143.5, 143.4, 133.6, 132.5, 132.1, 131.8, 131.5, 131.4, 129.3, 129.0, 128.0, 128.0, 127.9, 127.8, 127.7, 126.9, 126.8, 126.6, 126.5, 125.6, 118.9, 115.0, 77.4, 77.2, 76.9, 60.5, 31.3, 31.1, 27.6, 21.2, 17.8, 14.3, 0.1. HRMS (*m/z*): calcd for $C_{34}H_{29}NS$, 483.202; found, 483.202 (Supporting Information).

2.2. UV-Vis absorption and fluorescence spectroscopic methods

A spectrophotometer (Agilent Technologies Cary 8454, USA) was used to obtain the UV-Vis absorption spectra. A spectrofluorophotometer (Shimadzu corp. RF-6000, Kyoto, Japan) with a 10 mm standard quartz cell was used for the emission spectra acquisition. The compounds stock solution was prepared in dimethyl sulfoxide (DMSO, 10 mM). Photophysical properties of **AgP-1** (10 μM) were analyzed in various solvents (deionized water; DI H_2O, phosphate-buffered saline; PBS, ethanol; EtOH, ethyl acetate; EA, acetonitrile; ACN, tetrahydrofuran; THF, dimethyl sulfoxide; DMSO) at 25 °C. An aggregation-induced emission spectrum of **AgP-1** was measured in the glycerol-water mixture (pH 7.4, fraction from 0 to 50% (*v/v*)) at 25 °C.

2.3. DLS measurement

The hydrodynamic size of **AgP-1** and its silver ion complex were measured in buffer solution (pH 7.4) at 25 °C using Malvern Instruments Zetasizer Nano ZS90 (Worcester-shire, UK).

2.4. UV-vis titration of **AgP-1** with silver ions

3 μL of **AgP-1** (10 mM, DMSO) was added in 1 mL pH 7.4 buffer solution, and the UV-vis spectrum was measured. 3 μL of silver ions (333 μM, pH 7.4 buffer solution) was added then and mixed using a vortex mixer. After mixing, UV-vis spectrum was measured adding silver ion solution up to saturation.

2.5. DFT Calculation

Density functional theory (DFT) calculations were performed using the Gaussian 16W program package [26]. The ωB97XD functional, corresponding to Grimme's D2 dispersion model [27], was used with 6-31++G(d,p) basis set [28, 29] for all atom types except for Ag^{+}, for which the LANL2DZ effective core potential (ECP) was used [30, 31]. All calculations were performed using the integral equation formalism variant of a polarizable continuum model (IEFPCM) of water [32]. Input file and image generation were performed using Gaussview 6.0 [33].

2.6. Cell culture

U87MG cell line was obtained from American Type Culture Collection (ATCC, Manassas, VA, USA). The cells were cultured in Dulbecco's modified Eagle's media (DMEM, Hyclone, USA) supplemented with 10% fetal bovine serum (FBS, Hyclone, USA) and 1% penicillin-streptomycin (PS, Hyclone, USA) at 37 °C in a 5% CO_2 environment.

2.7. CLSM imaging of cells

U87MG cells (2×10^5 cells/mL) were seeded on 35-mm glass-bottom confocal dishes (SPL Life Science, Rep. of Korea) and incubated for 48 h at 37 °C. Cells were treated with **AgP-1** (40 μM, 2 h incubation) and $AgNO_3$ (40 μM, 10 min incubation). The cells were then stained with cell membrane staining reagent (1000×, CellMask Deep Red, Thermo Fisher, USA) for 10 min followed by PBS washing. A confocal laser scanning microscope (CLSM, Carl-Zeiss LSM 800 Exciter, Germany) was used to obtain fluorescence cellular images. Wavelength information

(excitation wavelength, emission channel); blue channel (405 nm, 410–650 nm), red channel (640 nm, 650–700 nm).

2.8. Cell viability assay

U87MG cells (5×10^4 cells) were seeded on a 96-well clear bottom plate (SPL Life Science, Rep. of Korea) and incubated for 24 h at 37 °C. After incubation, the cells were treated with DMSO (control) and **AgP-1** respectively and incubated for 2 h. The cell viability was analyzed with Vybrant MTT Cell Proliferation Assay Kit (ThermoFisher, USA) according to the manufacturer's instructions. The absorbance was analyzed at 550 nm with Spectra Max Gemini EM microplate reader (SpectraMax Gemini EM, Molecular Devices, US).

2.9. Bacteria culture

All bacterial strain-related studies were conducted in certified BSL-level facilities at Kyung Hee University Medical Center (Seoul, Republic of Korea). Strains of drug-sensitive bacteria (*staphylococcus aureus*; *S. aureus*) were obtained from the American Type Culture Collection (ATCC, USA) and the Culture Collection of Antibiotic-Resistant Microbes (CCARM, Republic of Korea). All bacterial strains were stored in skimmed milk and frozen at −70 °C. The bacterial strains were sub-cultured twice in cation-adjusted Mueller-Hinton broth (CA-MHB) for 24 h at 37 °C.

2.10. CLSM imaging of bacterials

The bacteria were cultured in CA-MHB overnight at 37 °C until reaching the exponential phase. After the overnight incubation, the cultured bacteria were harvested using a 1.5 mL microtube and centrifuged at 10,000×g for 5 min. The supernatants were discarded, and the bacteria pellets were resuspended/washed with buffer (PBS buffer, pH 7.4, three times). The washed bacteria pellets were re-suspended in PBS (pH 7.4) and incubated with **AgP-1** (40 μM, 2 h incubation) and $AgNO_3$ (40 μM, 10 min incubation) at 37 °C. After that, the bacteria were thoroughly washed with PBS (pH 7.4) and smeared on a slide glass for observation by confocal laser scanning microscopy (CLSM, Carl-Zeiss LSM 700 Exciter, Germany). Wavelength information (excitation wavelength, emission channel); blue channel (405 nm, 400–650 nm).

2.11. Minimum Inhibitory Concentration (MIC) Assay

MIC was determined using broth microdilution in CA-MHB according to the Clinical and Laboratory Standard Institute (CLSI, 2016) guidelines. Strains *staphylococcus aureus* bacteria were incubated with **AgP-1** (1.56–100 μM) using CA-MHB broth in a 96-well microplate for 24 h at 37 °C. The turbidity of all the strains was adjusted to a 0.5 McFarland standard (1×10^8 CFU/mL) and 10 μL of bacterial suspension was added to each well of a 96-well microplate, with the final concentration of each strain being approximately 5×10^5 CFU/mL.

3. Results and Discussion

3.1. Design and synthesis of **AgP-1**

In 2019, our group reported a fluorescent probe for the detection of iron(III) ions based on electron donor (D)-acceptor (A) type dipolar dye and 2-(methylthio)aniline Schiff based moiety (**FeP-1**, Type 1, Fig. 1b). As a follow-up research, we have focused on the development of a new fluorescent probe based on the tetraphenylethylene (TPE) and MTA moiety based on the secondary amine formation (Type 2 method).

TPE is one of the most widely used AIEgen because it is easy to (i) synthesize various derivatives and, (ii) regulate its photophysical properties in both solid-state and solution-state [34-36]. Generally, such TPE-based fluorescent probe shows an off-emission when fully dissolved in the solutions and an on-emission when aggregated in the solutions [37-39]. During the probe designing stage, we expected that **AgP-1** showed emission in aqueous media because it could be aggregated, and the emission decreased after **AgP-1** chelated with metal ions. During the characterization of **AgP-1**, however, we found that **AgP-1** existed as a nano-aggregate in aqueous media (see dynamic light scattering (DLS) measurement below) and had an off-emission of TPE due to the non-radiative pathway generation via the free-rotation of MTA moiety and non-efficient stacking (freely rotatable benzene rings) of TPE fluorophore. In the metal screening analysis, the high specificity of **AgP-1** towards silver ions was observed with significant emission enhancement due to the restricted rotation of MTA moiety via (i) silver ion chelation and (ii) increased stacking efficiency of TPE. We systematically conducted in vitro sensing ability assay of **AgP-1** with quantum mechanical calculations to understand the silver chelation mode. To verify the practical

applications of **AgP-1**, we used the confocal laser scanning microscopy (CLSM) for the imaging of silver ions within cancer cells (U87 glioblastoma) and bacteria (*S. aureus*).

AgP-1 was synthesized using 1-(bromomethyl)-4-(1,2,2-triphenylethenyl)benzene, 2-(methylthio)aniline in the presence of K_2CO_3 (base) and *N*,*N*-dimethylformamide (DMF) solvents (Fig. 2). The purity of the synthesized compound was confirmed by proton/carbon nuclear magnetic resonance ($^1H/^{13}C$ NMR), high-resolution mass spectrometry (HRMS), and attenuated total reflectance Fourier-transform infrared spectrum (ATR-FTIR) (data in ESI).

3.2. Sensing properties of **AgP-1**

First, the photophysical properties of **AgP-1** (10 μM) were demonstrated. In aqueous media (PBS buffer, pH 7.4), **AgP-1** displayed a major absorption peak at the wavelengths of 337 nm (Fig. 3a) and a weak emission peak at 474 nm (Fig. 3b) with a large Stokes shift in DI H_2O (153 nm) and PBS (140 nm) (Table S2) [40]. **AgP-1** showed no fluorescence in low-viscosity organic solvents such as ethanol (EtOH), ethyl acetate (EA), acetonitrile (ACN), tetrahydrofuran (THF), dimethyl sulfoxide (DMSO) with slight Stokes shift (Fig. S2, Table S2). The fluorescence quantum yield (QY, Φ) of **AgP-1** was also measured in each solvent (PBS buffer (pH 7.4), DI H_2O) and corresponded with these results; **AgP-1** in PBS buffer (Φ = 0.060) and **AgP-1** in DI H_2O (Φ = 0.089), as evidenced in comparison to the 9,10-diphenylanthracene (DPA) as a reference dye (Table S2). However, in high-viscosity solvents such as glycerol which induced aggregation of **AgP-1**, **AgP-1** shows enhanced emission as a ratio of glycerol increased (Fig. S3). This result indicates that **AgP-1** maintains the aggregation-induced emission of the TPE backbone, which leads to increased fluorescence intensity in high-viscosity solvents due to the restricted rotational freedom. We also monitored the pH effect of **AgP-1** throughout various pH values (pH 4, pH 5, pH 6, pH 7, and pH 7.4). Although the **AgP-1** showed increased fluorescence intensity in acidic conditions (pH 4, 5) due to the protonation of the amino group, non-significant photophysical changes in pH 6–7.4 (Fig. S4).

Next, we measured the fluorescence intensity of **AgP-1** (10 μM) in aqueous media (PBS buffer, pH 7.4) with silver ions or silver nanoparticles (AgNPs). An enhancement of absorbance and emission (3.72-fold) was observed when **AgP-1** reacted with silver ions and silver nanoparticles (Fig. 3a, 3b, Fig. S5). These results also supported the high sensitivity of **AgP-1**,

which could detect small amounts of dissolved silver ions from nanoparticles. The silver ion selectivity of **AgP-1** was evaluated by measuring the fluorescence intensity changes after adding various metal ions. A significant fluorescence increase was observed only for the silver ions. Although negligible response or slight interference ($AlCl_3$, $CuCl_2$, $ZnCl_2$, and $HgCl_2$) from metal ions or biologically abundant molecules showed, there were no considerable interferences to identify the silver ions (Fig. 3c). We further analyzed that selectivity toward silver ion of **AgP-1** with co-incubated with metal ions and biomolecules and confirmed that enhanced fluorescence intensity of **AgP-1** and silver ion complex was not interfered by other metal ions except for Pd^{2+} and Au^{3+}, which could result in fluorescence quenching (Fig. S6). To verify the high selectivity of **AgP-1** toward silver ion, we calculated the binding constant by the Benesi–Hildebrand plots and obtained the binding constant of **AgP-1** ($0.287 \times 10^{-1}M^{-1}$ in aqueous media) (Fig. S7). The binding ratio **AgP-1** with silver ion was analyzed using HR-mass spectra measurement (binding ratio; 1:1, calculated 590.1, found 590.2) (Fig. S8). We expected that the silver ion could make chelation with heteroatoms (N atom, S atom) in MTA and that such complex formation suppressed the free rotation of MTA moiety and phenyl rings within the TPE fluorophore which led to fluorescence enhancement. To understand such chelation formation, we measured the size changes of nano-aggregates after adding silver ions to the solution containing **AgP-1**. In the dynamic light scatting (DLS) analysis, the hydrodynamic diameter of **AgP-1** was 380.7 d.nm (polydispersity index (PDI): 0.346) and was enlarged to 522.6 d.nm (PDI: 0.328) when it formed a complex with silver ions (Fig. 3d). We think that the DLS data represent a silver complex formation of **AgP-1** and that its complex maintains the nano-size in aqueous media.

In a concentration-dependent assay of silver ions (0–300 μM), the fluorescence intensity of **AgP-1** increased with the increasing concentration of silver ions (Fig. 4a). In the low concentration of silver ions, it has appeared the detection limit of **AgP-1** toward silver ions is 0.312 μM (6.6 ppb), displaying a high sensitivity (Fig. 4b). The time-dependent emission intensity changes of **AgP-1** with silver ions were monitored in aqueous media (PBS buffer, pH 7.4). As shown in Fig. 4c, when silver ions are added to the **AgP-1** solution, a dramatic fluorescence enhancement was immediately observed within 10 s, proving that the TPE and MTA moiety-based approach using **AgP-1** is faster than the reported reaction-based probes.

Next, we conducted a silver ion sensing assay of **AgP-1** in the presence of ethylenediaminetetraacetic acid (EDTA), which has a high binding affinity for silver ions, to verify

whether the fluorescence enhancement of **AgP-1** is induced by silver ion chelation. As we expected, fluorescence enhancement of **AgP-1** was not high in the EDTA-containing silver ion solution (Fig. 4d, set: +EDTA + Ag^+), and the post-treatment of EDTA to the solution containing the complex of **AgP-1** and silver ions decreased the fluorescence intensity of **AgP-1** (Fig. 4d, set: +Ag^+ + EDTA). These results confirmed that the fluorescence enhancement of **AgP-1** was induced solely by the complex formation with silver ions.

3.3. DFT calculation

DFT calculations were performed on a discrete **AgP-1** and the corresponding silver complex using a dispersion corrected DFT functional. As expected, in the absence of silver ions, the HOMO and LUMO orbitals of **AgP-1** were fully centered on the tetraphenylethylene moiety (Fig. 5), which is consistent with a π–π* transition responsible for both excitation and emission behavior of **AgP-1**. A complex was formed in the presence of silver ions, in which the metal ion was coordinated by both the nitrogen and sulfur heteroatoms, and further electrostatic interactions (likely cation-π interactions) with two phenyl groups were observed as well. In line with the experimentally observed fluorescence enhancement, this type of complex would significantly reduce molecular motion disabling the rotation-enhanced fluorescence inhibition. Importantly, the HOMO and LUMO orbitals were still fully located on the tetraphenylethylene moiety and HOMO and LUMO energies have not significantly been altered. This is consistent with the identical maximum absorbance and emission wavelength of **AgP-1** and its silver ion complex.

Only a discrete 1:1 complex was calculated to avoid expensive calculations. Despite the slightly bent phenyl ring structure (approximately 4.6° deviation from planarity), the proposed complex structure was more favorable compared to a fully extended isomer where the silver ion only interacts with two heteroatoms. The complex of **AgP-1** and Ag^+ demonstrated the bond length between heteroatoms and the silver cation of 2.49 and 2.76 Å for the Ag-N and Ag-S bonds respectively, and distance between the benzene centroids and the metal ion of 3.04 and 3.27 Å, which is significantly shorter than the generally accepted cutoff of 6 Å for cation – π interactions (Fig. S9). As both **AgP-1** and the **AgP-1** + Ag^+ complex form aggregates in solution, an extended conformation, instead of a 1:1 complex, is nonetheless adopted for the silver complex where it is further stabilized by cation-π interactions with a silver ion bound by an adjacent compound. However, regardless of the interaction mode, these calculations strongly support the formation of

a rigidified scaffold after adding silver, resulting in a stronger AIEgen effect and enhanced fluorescence intensity without significant alteration of the emission wavelength.

3.4. CLSM imaging of silver ions in cancer cells

With the promising in vitro analysis result, we analyzed the silver ion sensing ability of **AgP-1** maintained in the biological environment for further application to detect remaining silver ions within anticancer drugs [41]. Before the cell study, we measured the hydrodynamic size of **AgP-1** in cell culture media to confirm the colloidal stability. The hydrodynamic diameter of **AgP-1** was 205.4 d.nm (PDI: 0.307), and it was maintained for 1 h (after incubation: 205.6 d.nm, PDI: 0.294) (Fig. S10). After confirming the colloidal stability of **AgP-1** in culture media, **AgP-1** was applied to the bioimaging of silver ions in cancer cells (U87MG, glioblastoma cells) (Fig. 6). In the absence of **AgP-1**, there was no background fluorescence in confocal laser scanning microscopy (CLSM). When U87MG cells were incubated with **AgP-1** (40 μM), weak fluorescence signals were observed in the detection channel (450–650 nm) at cellular cytosol (Fig. 6a, top, left). To confirm the sensing ability of **AgP-1** for silver ions in the cells, U87MG cells were pre-incubated with silver ions (40 μM), followed by **AgP-1** (40 μM), and then it was fixed for CLSM imaging after thorough washing with PBS buffer (pH 7.4). As shown in Fig. 6a (top, right) and Fig. 6b, a bright fluorescence signal was observed in the same detection channel at cellular cytosol, and such promising results revealed the sensing ability of **AgP-1** for silver ions in a biological environment. We also co-treated a cell membrane staining reagent (Cell-mask Deep-red) to observe the cell membrane in cellular cytosol, and the results showed that **AgP-1** reacted with silver ions in cytosol. In the cell viability analysis, **AgP-1** showed negligible cytotoxicity even at high concentrations (~80 μM) (Fig. 6c), which represents the high biocompatibility of **AgP-1**.

3.5. CLSM imaging of silver ions in *S. aureus*

Further bioimaging applications of **AgP-1** were conducted in the bacteria strain of *staphylococcus aureus* (*S. aureus*) (Fig. 7) as silver ions have been widely used in the biological study of bacteria strains for the antibiotic development and the drug-related mechanism study. When *S. aureus* was treated with **AgP-1** (40 μM), a negligible fluorescence signal was observed in the CLSM imaging views (Fig 7a, middle), but bright fluorescence images appeared in the pre-treated set of silver ions

(40 μM) (Fig. 7a, left), which is a similar result (significant fluorescence enhancement in the set of **AgP-1** + silver ions; Fig. 7b) to the CLSM cell imaging results. Such application supports the promising possibility of using **AgP-1** for the detection of silver ions within bacteria. In the minimum inhibitory concentration (MIC) level toward *S. aureus* analysis, **AgP-1** showed no growth inhibition of the *S. aureus* strains even at high concentrations (200 μM), which indicates that **AgP-1** has a promising potential for application within live *S. aureus* (Fig. S11).

4. Conclusion

In this study, we developed a new fluorescent nanoprobe (**AgP-1**) for the detection of silver ions based on a hybridized structure of AIEgen (tetraphenylethylene; TPE) and 2-(methylthio)aniline (MTA) moiety via secondary amine formation. **AgP-1** showed an increased fluorescence intensity when making a complex with silver ion in biological media through the restricted rotation of MTA moiety by silver ion chelation and the increased stacking of TPE structure. **AgP-1** displayed high selectivity for silver ions without interfering with the metal ions or biomolecules and showed excellent detecting ability (detection limit: 6.6 ppb) and a fast response time (within 10 s). In addition, **AgP-1** displayed high biocompatibility with low toxicity toward U87MG (glioblastoma cells) and visualizing ability of silver ion in cancer cells (U87MG) and bacteria (*S. aureus*). We expect this newly developed fluorescent nanoprobe to serve as a powerful tool for silver-related chemical research and biological studies.

Acknowledgments

This research was supported by the Basic Science Research Program through the National Research Foundation (NRF) of Korea funded by the Ministry of Education (NRF-2018-R1A6A1A03025124, NRF-2018-R1D1A1B07043383; D. K.) and the Bio & Medical Technology Development Program of the NRF of Korea funded by the Ministry of Science & ICT (NRF-2019-M3A9H1103783; D. K.). This research was also supported by a grant from the Korea Health Technology R&D Project of the Korea Health Industry Development Institute (KHIDI) funded by the Ministry of Health & Welfare, Republic of Korea (grant number: HI21C0239; D. K.) and the Bio & Medical Technology Development Program of the NRF of Korea (NRF-2021-

M3A9I5030523; D. K.). This research was also supported by Interne Fondsen KU Leuven / Internal Funds KU Leuven (STG/19/029; P. V.).

Appendix

Supplementary data related to this article can be found in the web version.

References

[1] Fu L, Wang A, Xie K, Zhu J, Chen F, Wang H, et al. Electrochemical detection of silver ions by using sulfur quantum dots modified gold electrode. Sens. Actuators B Chem. 2020;304:127390.
[2] Han Q, Liu X, Wang X, Song Y, Yang L, Li J, et al. Photoactivated fluorescence-based analysis for the facilitative and selective detection of silver (I) in aqueous solutions. Dyes Pigm. 2021;184:108793.
[3] Li Y, Yuan J, Xu Z. A Sensitive Fluorescence Biosensor for Silver Ions (Ag+) Detection Based on C-Ag+-C Structure and Exonuclease III-Assisted Dual-Recycling Amplification. J. Anal. Methods Chem. 2019;2019.
[4] Liu C, Wei X, Hao S, Zong B, Chen X, Li Z, et al. Label-Free, Fast Response, and Simply Operated Silver Ion Detection with a Ti3C2T x MXene Field-Effect Transistor. Anal. Chem. 2021.
[5] Galdiero S, Falanga A, Vitiello M, Cantisani M, Marra V, Galdiero M. Silver nanoparticles as potential antiviral agents. Mol. 2011;16(10):8894-918.
[6] Balasubramaniam B, Prateek, Ranjan S, Saraf M, Kar P, Singh SP, et al. Antibacterial and antiviral functional materials: Chemistry and Biological Activity toward Tackling COVID-19-like Pandemics. ACS Pharmacol. Transl. Sci. 2020;4(1):8-54.
[7] Talarska P, Boruczkowski M, Żurawski J. Current Knowledge of Silver and Gold Nanoparticles in Laboratory Research—Application, Toxicity, Cellular Uptake. Nanomaterials. 2021;11(9):2454.
[8] Charehsaz M, Hougaard KS, Sipahi H, Ekici AID, Kaspar Ç, Culha M, et al. Effects of developmental exposure to silver in ionic and nanoparticle form: A study in rats. DARU J. Pharm. Sci. 2016;24(1):1-13.
[9] Lu Z, Liu Y, Lu S, Li Y, Liu X, Qin Y, et al. A highly selective TPE-based AIE fluorescent probe is developed for the detection of Ag+. RSC Adv. 2018;8(35):19701-6.
[10] Mahajan R, Kumar M, Sharma V, Kaur I. Silver (I) ion-selective membrane based on Schiff base–p-tert-butylcalix [4] arene. Analyst. 2001;126(4):505-7.
[11] Shamsipur M, Kazemi SY, Niknam K, Sharghi H. A new PVC-membrane electrode based on a thia-substituted macrocyclic diamide for selective potentiometric determination of silver ion. Bull. Korean Chem. Soc. 2002;23(1):53-8.
[12] de Souza FC, Vegas CG, da Silva DAI, Ribeiro MS, Cabral MF, de Melo MA, et al. Amperometric and potentiometric determination of iodide using carbon electrodes modified with salophen complex. J. Electroanal. Chem. 2016;783:49-55.
[13] Qu W-J, Fang H, An J-N, Yang H-H, He J-X, Yao H, et al. Highly sensitive detection of mercury (II) and silver (I) ions in aqueous solution via a chromene-functionalized imidazophenazine derivative. J. Photochem. Photobiol. A: Chem. 2020;402:112814.
[14] Arulraj AD, Devasenathipathy R, Chen S-M, Vasantha VS, Wang S-F. Highly selective and sensitive fluorescent chemosensor for femtomolar detection of silver ion in aqueous medium. Sens. Bio-Sens. Res. 2015;6:19-24.
[15] Kim J, Lee S, Kim S, Jung M, Lee H, Han MS. Development of a fluorescent chemosensor for chloride ion detection in sweat using Ag+-benzimidazole complexes. Dyes Pigm. 2020;177:108291.
[16] Yin G, Yu T, Niu T, Yin P, Chen H, Zhang Y, et al. A novel fluorescence turn-on probe for the selective detection of thiophenols by caged benzooxazolidinoindocyanine. RSC Adv. 2017;7(73):46148-54.
[17] Giovannini G, Gubala V, Hall AJ. 'Off–on'switchable fluorescent probe for prompt and cost-efficient detection of bacteria. New J. Chem. 2019;43(33):13094-102.

[18] Gu B, Huang L, Hu J, Liu J, Su W, Duan X, et al. Highly selective and sensitive fluorescent probe for the detection of nitrite. Talanta. 2016;152:155-61.
[19] Li Z, Chen W, Dong L, Song Y, Li R, Li Q, et al. A novel ratiometric and reversible fluorescent probe based on naphthalimide for the detection of Al 3+ and pH with excellent selectivity. New J. Chem. 2020;44(8):3261-7.
[20] Kim MS, Jo TG, Ahn HM, Kim C. A colorimetric and fluorescent chemosensor for the selective detection of Cu 2+ and Zn 2+ Ions. J. Fluoresc. 2017;27(1):357-67.
[21] Sivaraman G, Anand T, Chellappa D. Development of a pyrene based "turn on" fluorescent chemosensor for Hg 2+. RSC Adv. 2012;2(28):10605-9.
[22] Yang L, Song Q, Damit-Og K, Cao H. Synthesis and spectral investigation of a Turn-On fluorescence sensor with high affinity to Cu2+. Sens. Actuator B-Chem. 2013;176:181-5.
[23] Suganthi G, Sivakolunthu S, Ramakrishnan V. Solvatochromic and preferential solvation studies on Schiff base 1, 4-Bis (((2-methylthio) phenylimino) methyl) benzene in binary liquid mixtures. J. Fluoresc. 2010;20(6):1181-9.
[24] Kim NH, Lee J, Park S, Jung J, Kim D. A schiff base fluorescence enhancement probe for Fe (III) and its sensing applications in cancer cells. Sensors. 2019;19(11):2500.
[25] Tharmaraj V, Devi S, Pitchumani K. An intramolecular charge transfer (ICT) based chemosensor for silver ion using 4-methoxy-N-((thiophen-2-yl) methyl) benzenamine. Analyst. 2012;137(22):5320-4.
[26] Frisch MJ, Trucks GW, Schlegel HB, Scuseria GE, Robb MA, Cheeseman JR, et al. Gaussian 16 Rev. C.01. Wallingford, CT2016.
[27] Chai J-D, Head-Gordon M. Long-range corrected hybrid density functionals with damped atom–atom dispersion corrections. Phys. Chem. Chem. Phys. 2008;10(44):6615-20.
[28] Clark T, Chandrasekhar J, Spitznagel GW, Schleyer PVR. Efficient diffuse function-augmented basis sets for anion calculations. III. The 3-21+ G basis set for first-row elements, Li–F. J. Comput. Chem. 1983;4(3):294-301.
[29] Frisch MJ, Pople JA, Binkley JS. Self-consistent molecular orbital methods 25. Supplementary functions for Gaussian basis sets. J. Chem. Phys. 1984;80(7):3265-9.
[30] Hay PJ, Wadt WR. Ab initio effective core potentials for molecular calculations. Potentials for the transition metal atoms Sc to Hg. J. Chem. Phys.1985;82(1):270-83.
[31] Hay PJ, Wadt WR. Ab initio effective core potentials for molecular calculations. Potentials for K to Au including the outermost core orbitals. J. Chem. Phys. 1985;82(1):299-310.
[32] Tomasi J, Mennucci B, Cammi R. Quantum mechanical continuum solvation models. Chem. Rev. 2005;105(8):2999-3094.
[33] Dennington R, Keith TA, Millam JM. GaussView, version 6.0. 16. Semichem Inc Shawnee Mission KS. 2016.
[34] Mei J, Leung NL, Kwok RT, Lam JW, Tang BZ. Aggregation-induced emission: together we shine, united we soar! Chem. Rev. 2015;115(21):11718-940.
[35] Mei J, Hong Y, Lam JW, Qin A, Tang Y, Tang BZ. Aggregation-induced emission: the whole is more brilliant than the parts. Adv. Mater. 2014;26(31):5429-79.
[36] Hong Y, Lam JW, Tang BZ. Aggregation-induced emission. Chem. Soc. Rev. 2011;40(11):5361-88.
[37] Zhang S, Huang Y, Kong L, Zhang X, Yang J. Aggregation-induced emission-active tetraphenylethylene derivatives containing arylimidazole unit for reversible mechanofluorochromism and selective detection of picric acid. Dyes Pigm. 2020;181:108574.

[38] Hu Q, Huang Q, Liang K, Wang Y, Mao Y, Yin Q, et al. An AIE+ TICT activated colorimetric and ratiometric fluorescent sensor for portable, rapid, and selective detection of phosgene. Dyes Pigm. 2020;176:108229.
[39] Kim NH, Kim BW, Moon H, Yoo H, Kang RH, Hur JK, et al. AIEgen-based nanoprobe for the ATP sensing and imaging in cancer cells and embryonic stem cells. Anal. Chim. Acta. 2021;1152:338269.
[40] Xu J, Xiong J, Qin Y, Li Z, Pan C, Huo Y, et al. A novel quinolinyl-tetraphenylethene-based fluorescence “turn-on” sensor for Zn 2+ with a large Stokes shift and its applications for portable test strips and biological imaging. Mater. Chem. Front. 2020;4(11):3338-48.
[41] Greulich C, Braun D, Peetsch A, Diendorf J, Siebers B, Epple M, et al. The toxic effect of silver ions and silver nanoparticles towards bacteria and human cells occurs in the same concentration range. RSC Adv. 2012;2(17):6981-7.

Figures

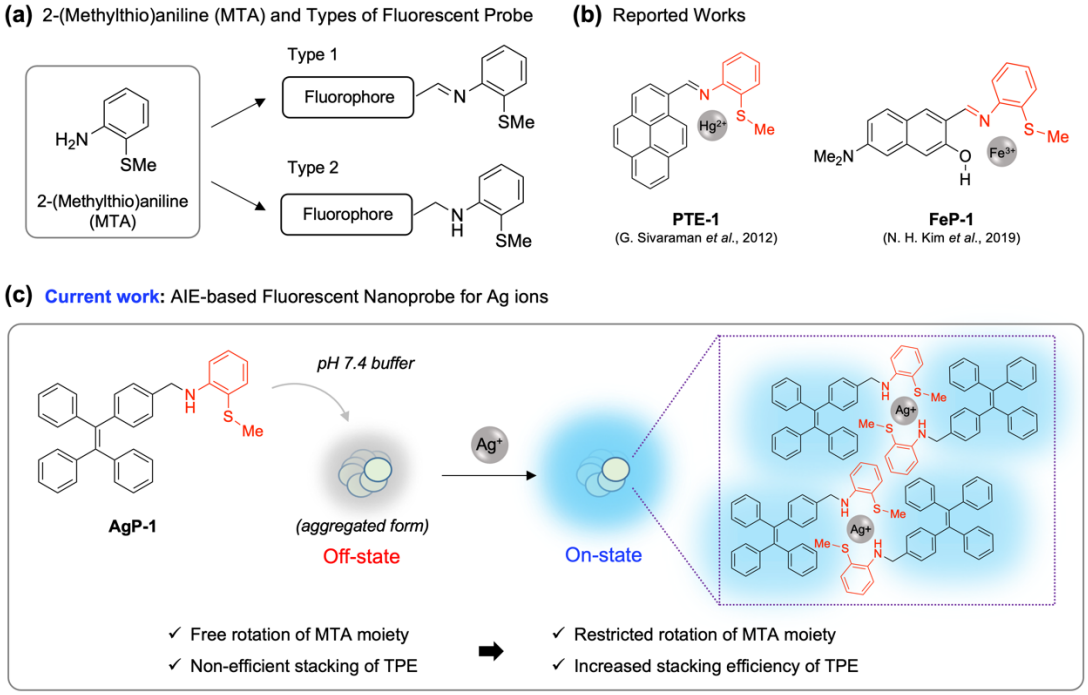

Fig. 1. (a) Chemical structure of 2-(Methylthio) aniline and the existing approaches (types) for developing the fluorescent probe based on MTA moiety. (b) Existing Work: fluorescent probes for mercury (Hg^{2+}) and iron (Fe^{3+}) based on the 2-(Methylthio) aniline Schiff moiety. (c) Current work: AIE-based fluorescent nanoprobe (**AgP-1**) for silver ions and its schematic illustration of the working mechanism.

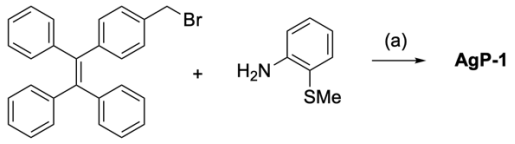

Fig. 2. Synthetic scheme of **AgP-1**. Reagents and conditions: (a) K_2CO_3, DMF, 80 °C, 12 h, yield 30%.

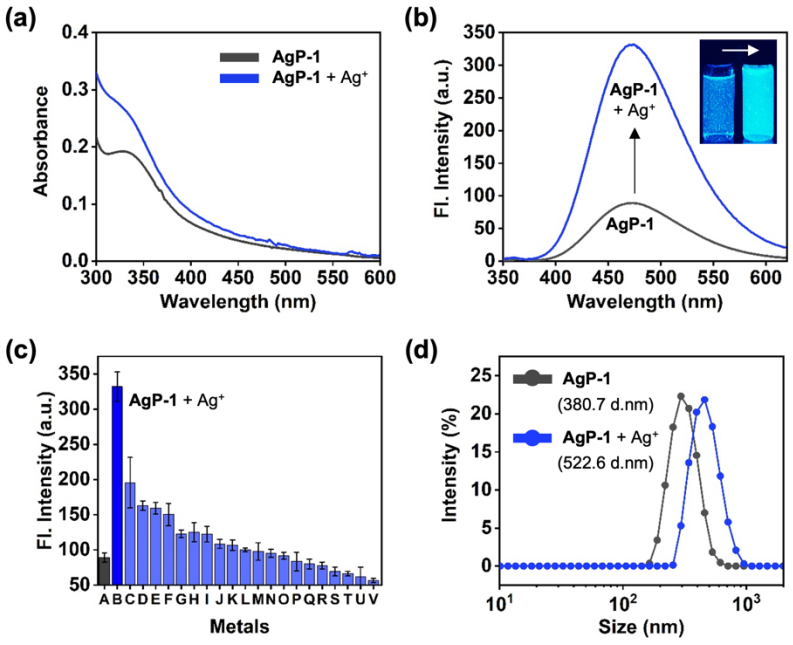

Fig. 3. (a) Absorption and (b) emission spectra of **AgP-1** (10 μM) after adding Ag ions (30 eq) in aqueous solution (PBS buffer, pH 7.4). The spectra were recorded within 10 s of mixing at 25 °C under excitation at 337 nm. Inset: photos of **AgP-1** (10 μM) in aqueous solution before and after treatment with Ag ions (30 eq) under UV light (365 nm). (c) Emission intensity plot (peak height at 474 nm) of **AgP-1** (10 μM) after adding various metal ions (30 eq) to aqueous solution (PBS buffer, pH 7.4). The spectra were recorded within 10 s of mixing at 25 °C under excitation at 337 nm. (A) **AgP-1** (10 μM), (B) $AgNO_3$, (C) $AlCl_3$, (D) $CuCl_2$, (E) $ZnCl_2$, (F) $HgCl_2$, (G) $MgCl_2$, (H) L-lysine, (I) L-gluthathione, (J) KCl, (K) DL-homocysteine, (L) L-gluthamine, (M) $CaCl_2$, (N) $CoCl_2$, (O) AuCl, (P) $NiCl_2$, (Q) L-cysteine, (R) $CdCl_2$, (S) $FeCl_3$, (T) $PdCl_2$, (U) $AuCl_3$, (V) $FeCl_2$. Means and standard deviations calculated from multiple measurements (n = 3). (d) The intensity distribution curves derived from the dynamic light scattering (DLS) measurement of **AgP-1** (10 μM) in aqueous solution (PBS buffer, pH 7.4). Polydispersity index (PDI): **AgP-1** (0.346), **AgP-1** + Ag^+ (0.328).

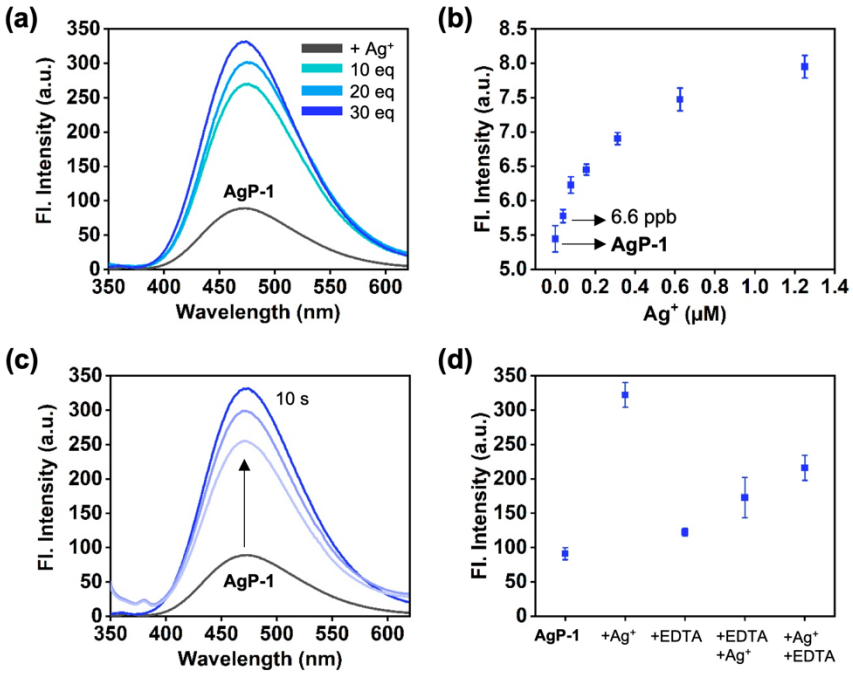

Fig. 4. (a) The emission spectrum of **AgP-1** (10 μM) after adding Ag ions (0–300 μM) in aqueous solution (PBS buffer, pH 7.4), measured after 10 s at 25 °C under excitation at 337 nm. (b) The plot of fluorescence intensity (peak height at 474 nm) of **AgP-1** (0.312 μM) after adding Ag ions (0–1.25 μM) in aqueous solution (PBS buffer, pH 7.4), measured after 10 s at 25 °C under excitation at 337 nm. (c) The time-dependent emission spectrum of **AgP-1** (10 μM) after adding Ag ions (30 eq) in aqueous solution (PBS buffer, pH 7.4), measured after 10 s at 25 °C under excitation at 337 nm. (d) The emission spectrum of **AgP-1** (10 μM) after adding it into EDTA (100 μM) with/without Ag ions (30 eq) in aqueous solution (PBS buffer, pH 7.4), measured after 10 s at 25 °C under excitation at 337 nm.

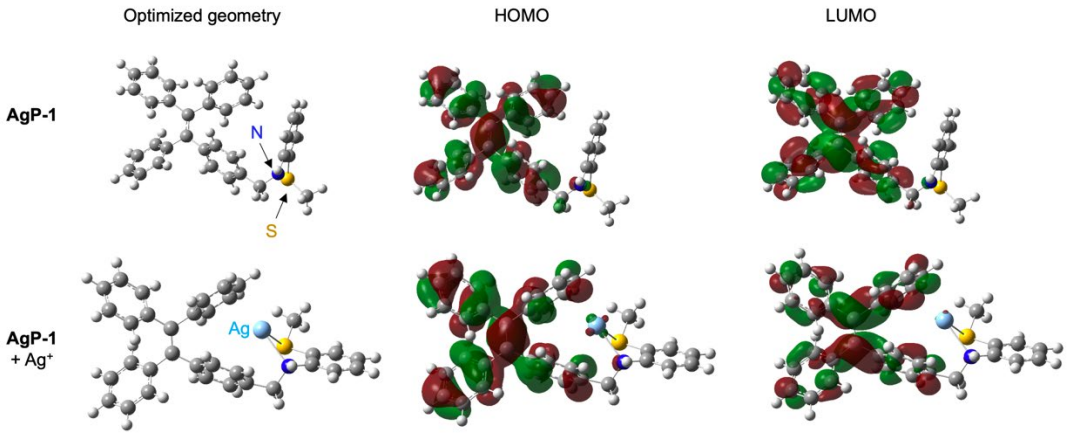

Fig. 5. Optimized geometry and HOMO/LUMO of **AgP-1** and its silver complex. Calculations were performed at the ωB97XD/6-31++G(d,p) level of theory using LANL2DZ effective core potential (ECP) for silver ions. Frontier orbitals are depicted at the 0.02 e/bohr^3 isodensity surface.

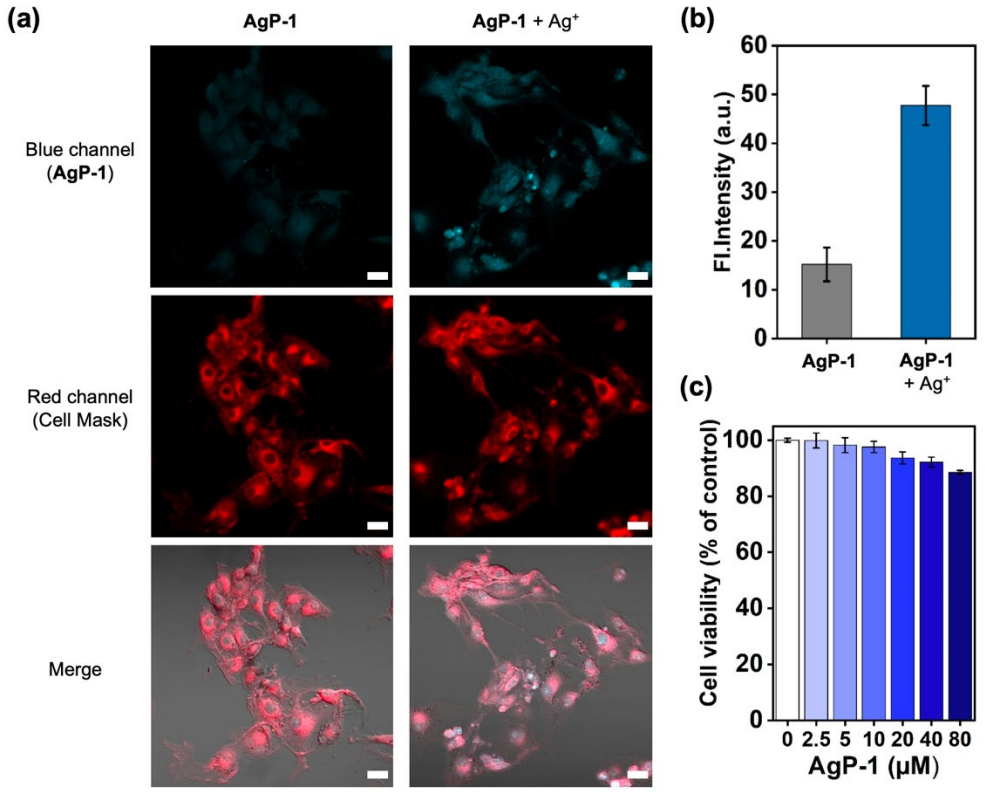

Fig. 6. (a) CLSM images of **AgP-1** in U87MG cells (magnification, ×20). [**AgP-1**]: cells with **AgP-1** (40 μM, incubation for 2 h at 37 °C); [**AgP-1**+Ag^{+}]: cells with **AgP-1** (40 μM, incubated for 2 h at 37 °C) and Ag ions (40 μM, incubated for 10 min at 37 °C). Cell-Mask Deep-red: 2 μL (1000× working concentration, incubated for 10 min at 37 °C). Scale bar: 20 μm. Blue channel: excitation wavelengths at 405 nm, emission channel at 400–650 nm. Red channel: excitation wavelengths at 640 nm, emission channel at 650–700 nm. Merged: a superimposed image of differential interference contrast (DIC), blue channel, and red channel. (b) The relative fluorescence intensity plots of cells in panel (a). The intensity in cells was measured using Image-J by drawing the ROI (region of interest) over the entire cells based on the fluorescence images. (c) Cell viability of **AgP-1**. Cells were incubated with 0–80 μM of **AgP-1** for 2 h at 37 °C. Experiments were performed in triplicate to calculate means and standard deviations.

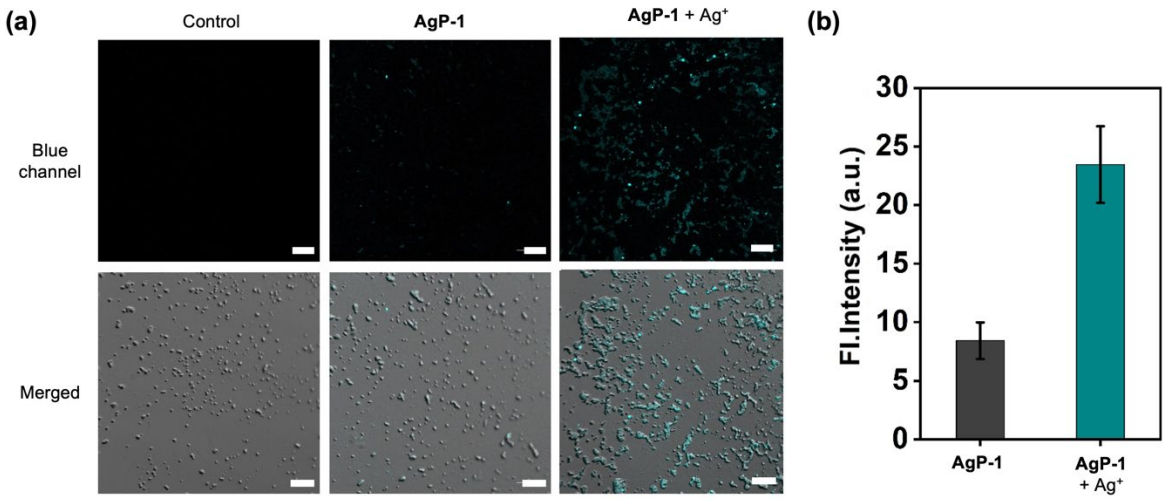

Fig. 7. (a) CLSM images of **AgP-1** (40 μM) in *staphylococcus aureus* (magnification: ×20). [**AgP-1**]: bacteria with **AgP-1** (40 μM, incubated for 2 h at 37 °C); [**AgP-1**+Ag^{+}]: bacteria with Ag ions (40 μM, incubated for 10 min at 37 °C) and further incubation with **AgP-1** (40 μM, incubated for 2 h at 37 °C). Blue channel: excitation wavelengths at 405 nm, emission channel at 400–650 nm. Merged: a superimposed image of DIC and blue channel. (b) The relative fluorescence intensity plots of bacteria in panel (a). The intensity in bacteria was measured using Image-J by drawing the ROI (region of interest) over the entire bacteria based on the fluorescence images. Experiments were performed in triplicate to calculate means and standard deviations.

TOC

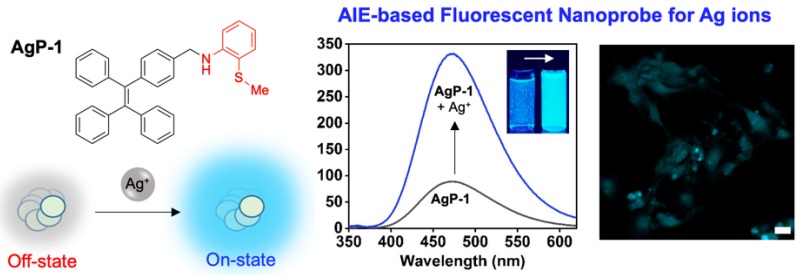
AgP-1
N
H
S
Me
Ag+
Off-state
On-state
AIE-based Fluorescent Nanoprobe for Ag ions
350
300
250
200
150
100
50
0
AgP-1
+ Ag+
AgP-1
350 400 450 500 550 600
Wavelength (nm)